Ultrafast dynamics in the power stroke of a molecular rotary motor

Conyard, Jamie; Addison, Kiri; Heisler, Ismael A.; Cnossen, Arjen; Browne, Wesley R.; Feringa, Ben L.; Meech, Stephen R.

Published in:
Nature Chemistry

DOI:
10.1038/NCHEM.1343

Publication date:
2012

nature chemistry

ARTICLES

PUBLISHED ONLINE: 6 MAY 2012 | DOI: 10.1038/NCHEM.1343

Ultrafast dynamics in the power stroke of a molecular rotary motor

Jamie Conyard[1], Kiri Addison[1], Ismael A. Heisler[1], Arjen Cnossen[2], Wesley R. Browne[2], Ben L. Feringa[2]* and Stephen R. Meech[1]*

Light-driven molecular motors convert light into mechanical energy through excited-state reactions. Unidirectional rotary molecular motors based on chiral overcrowded alkenes operate through consecutive photochemical and thermal steps. The thermal (helix inverting) step has been optimized successfully through variations in molecular structure, but much less is known about the photochemical step, which provides power to the motor. Ultimately, controlling the efficiency of molecular motors requires a detailed picture of the molecular dynamics on the excited-state potential energy surface. Here, we characterize the primary events that follow photon absorption by a unidirectional molecular motor using ultrafast fluorescence up-conversion measurements with sub 50 fs time resolution. We observe an extraordinarily fast initial relaxation out of the Franck–Condon region that suggests a barrierless reaction coordinate. This fast molecular motion is shown to be accompanied by the excitation of coherent excited-state structural motion. The implications of these observations for manipulating motor efficiency are discussed.

A detailed understanding of the factors that control the conversion of light into mechanical energy by light-driven molecular machines[1,2] is central to their efficient operation. In this work we probe the mechanism of the double-bond photoisomerization that underpins the operation of unidirectional molecular rotary motors, which were first reported by Feringa and co-workers in studies of chiral overcrowded alkenes (Fig. 1)[3–5]. These molecules comprise a 'rotor' (upper part) linked by an 'axle' (a double bond in the ground state) to a 'stator' (lower part), which may itself be linked to a larger structure, a surface for example[6]. An excited-state photoisomerization leads to a rotation of the rotor relative to the stator about the axle (the power stroke). The photochemical power stroke is followed by a second slower step in the electronic ground state, a thermal helix inversion, in which the configuration at the stereogenic centre leads to rotation with an overwhelming preference for one direction relative to the stator. A second pair of photochemical and thermal isomerization steps completes the cycle (Fig. 1)[5].

The efficiency of the thermal stroke was optimized through chemical synthesis, which has increased the rate by more than a factor of a million, and in principle allows the motors to operate at MHz rotation frequencies[7,8]. In contrast, rather little is known about the power stroke and how it depends on molecular structure and environment[9]. Control over this photoisomerization reaction is critical for the future exploitation of light-driven motors in molecular machines and devices. For example, optimization of isomerization over ground-state repopulation maximizes the use of optical power and minimizes the generation of deleterious local heating. To achieve this level of control requires knowledge of both molecular dynamics on the excited-state potential surface and of the coupling between the excited- and ground-state surfaces, which in turn requires measurements of the ultrafast dynamics; such a study is reported here.

One recent study[10] of ultrafast transient absorption in a molecular motor concluded that a structural relaxation within 1.7 ps was followed by an excited-state decay of 12 ps, a conclusion that was broadly supported by recent quantum mechanical and molecular dynamics calculations[11]. Here we apply ultrafast fluorescence up-conversion spectroscopy with a time resolution better than 50 fs (ref. 12) to probe the earliest excited-state dynamics of the molecular motor **1** (Fig. 1). Ultrafast fluorescence spectroscopy is uniquely suited to this objective because it unambiguously reveals information about excited-state dynamics, and preferentially probes the initially excited bright (Franck–Condon) region of the excited-state potential energy surface[13]. Here we resolve excited-state dynamics on the tens of femtoseconds timescale, and these dynamics are shown to be coupled with coherent low-frequency modes in the excited state. The implications of these observations for controlling the operational efficiency of light-driven motors are considered.

Results and discussion

Time-resolved fluorescence data. Figure 2a shows the electronic spectra for **1** in dichloromethane (DCM). The absorption (maximum at 390 nm) is narrow and well defined and quite characteristic of a substituted fluorene, which suggests the excitation is localized on the stator[14]. In contrast, the fluorescence spectrum, which is very weak (quantum yield estimated at $<10^{-4}$), is exceedingly broad, stretching from 350 nm to >750 nm with a maximum at 474 nm. Such a low yield and broad emission are characteristic of a molecule undergoing excited-state structural

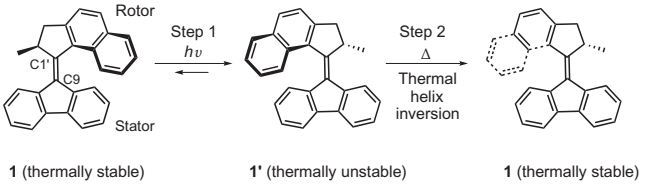

Figure 1 | Structure of the molecular motor 1. The three components, rotor–axle–stator, are indicated and the photochemical (power) and thermal strokes in the operation are shown. Further photoisomerization and thermal isomerization steps complete one cycle of the motor rotation.

[1]School of Chemistry, University of East Anglia, Norwich Research Park, Norwich NR4 7TJ, UK, [2]Stratingh Institute for Chemistry, University of Groningen, Nijenborgh 4, 9747AG Groningen, The Netherlands. *e-mail: s.meech@uea.ac.uk; b.l.feringa@rug.nl

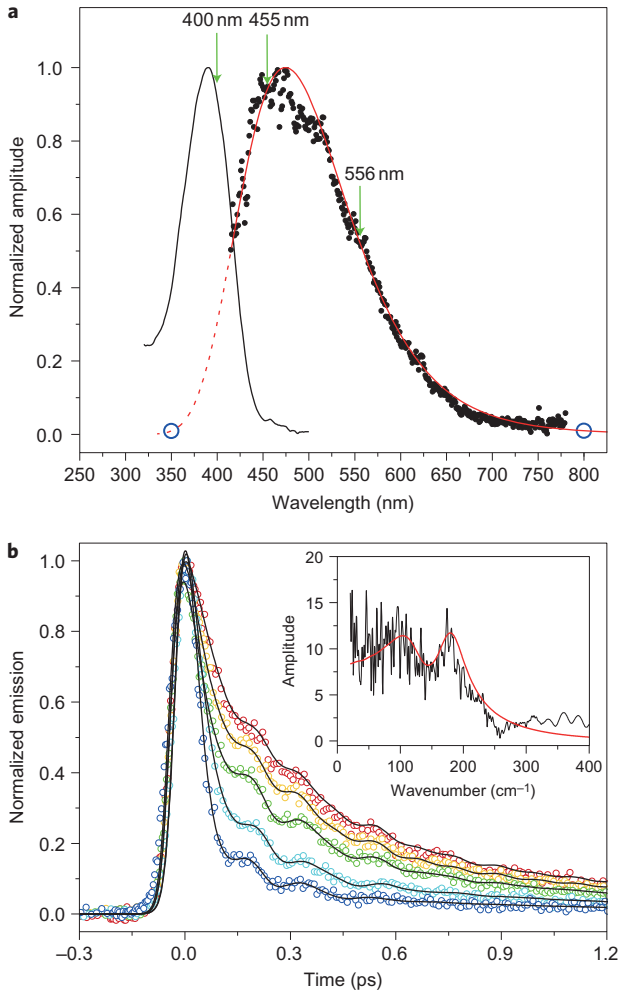

Figure 2 | Steady-state and time-resolved electronic spectroscopy of 1. **a**, Steady-state absorption and emission spectra in DCM. Data for the weak emission spectrum are black points, which were recovered after subtraction of the solvent Raman scattering. The fitted line is a log-normal function, and the blue circles indicate the assumed end points for the emission. Excitation and the range of emission wavelengths studied are shown by green arrows. **b**, Wavelength-resolved fluorescence up-conversion in DCM recorded across the emission spectrum. Points are data measured at 455 nm (dark blue), 472 nm (light blue), 535 nm (green), 545 nm (yellow), 556 nm (red) and the fitted functions are the black lines. Time-domain data were analysed by an evolutionary algorithm that minimized chi-square with the quality of fit judged by residual distribution; details of the analysis are given in Supplementary Section S1, Figs S1 and S2, and Tables S1 and S2. The inset shows the Fourier transform of the 535 nm time-domain data, with the exponential decay part subtracted. The Fourier transform of the experimental data (black line) is compared to that of the fitted data (red line). Contributions from two low-frequency modes are evident.

dynamics[15]. The measured time-resolved emission profiles for different wavelengths are shown in Fig. 2b. The decay on the higher energy side of the emission is extremely fast, which shows that the primary processes in these light-driven molecular motors occur within 100 fs. As the emission wavelength selected is tuned towards the red region the decay time lengthens. Superimposed on this ultrafast wavelength-dependent decay is a series of oscillations with maxima at approximately 170, 320 and 530 fs. Such oscillations in fluorescence-decay profiles are evidence of the excitation of coherent motion on the excited-state potential energy surface, and have implications for the optical coherent control of motor action[16,17]. The oscillatory part of the response is shown in the frequency domain as an inset in Fig. 2b, where it is evident that two modes contribute.

Each decay profile was fitted to a convolution of the instrument response (a Gaussian with 50 fs width) with a function that comprised a sum of two exponential relaxation terms and two damped harmonic oscillators. This was the minimum number of components required to achieve a good fit to the data shown (Fig. 2b). The fitting function and the resulting wavelength-dependent fitting parameters are collected in the Supplementary Information (Supplementary Figs S1 and S2). Both the fast- and slow-decaying components are a function of wavelength, with the dominant short component increasing from 110 fs at 455 nm to 290 fs at 556 nm (Supplementary Table S1). The minor (<20% amplitude) longer component increases from 0.9 ps to 1.5 ps over the same range. In contrast, the frequencies of the two harmonic oscillators are independent of wavelength within experimental error and are 3.4 ± 0.2 THz (113 ± 7 cm^{-1}) for the major oscillation and 5.4 ± 0.4 THz (180 ± 12 cm^{-1}) for the minor one (Supplementary Table S2). The width and relative weight of the two modes is illustrated in the Fourier transform of the oscillatory part of the 535 nm data (Fig. 2b inset). The amplitude of the higher-frequency oscillation in this case is 36% that of the lower-frequency one, but the relative amplitude is wavelength dependent, increasing from 20% to 40% between 455 and 576 nm. The damping constants for these modes are 95 ± 30 fs and 220 ± 50 fs, respectively, which corresponds with the lower-frequency mode in the Fourier transform with the greater width (Fig. 2b). Further details of the fitting procedure are given in Supplementary Section S1 and Figs S1 and S2.

To characterize properly the molecular dynamics on the excited-state potential surface it is necessary to recover the temporal evolution of the emission spectrum. This is achieved by area normalizing the wavelength-resolved deconvoluted decay functions to the intensity in the time-integrated emission spectrum (Fig. 2a). The resulting spectra are shown in Fig. 3a, where the data points are fitted to a log-normal line shape (complete information is given in Supplementary Section S2 and Fig. S3). As the spectra are much broader than the range that can be accessed by fluorescence up-conversion, the log-normal fits are constrained by assuming that the emission spectral intensity is zero at 350 nm and 800 nm, consistent with the steady-state spectrum (Fig. 2a). The temporal evolution of the fitted spectra is best represented by the contour plot in Fig. 3b. The time-dependent mean frequency, intensity (spectral area) and spectral width are shown in Fig. 3c.

Excited-state dynamics. The dominant feature in the time-dependent excited-state dynamics (Fig. 3) is the non-exponential decay in the integrated fluorescence intensity, which has an ultrafast (about 100 fs) component plus a slower decay on a picosecond timescale. This is accompanied by a continuous shift to lower wavenumber (red shift) of the emission spectra with time (Fig. 3b,c). The spectral shift arises from the ultrafast collapse of the emission on the blue edge of the spectrum (Fig. 2b). No rise time was detected on the red edge, such as that expected if polar solvent reorientation stabilized the excited state (solvation dynamics). Such a solvation red shift is, in any case, expected to be small in the relatively apolar solvent used, and essentially identical kinetics were observed for **1** in the apolar but more viscous solvent cyclohexane (data not shown). The lack of a viscosity effect is consistent with earlier measurements for which a very high viscosity was required to influence the photochemical equilibrium of a molecular motor[18]. Thus, we conclude that the rapid decay and red shift of the spectrum reflect intrinsic dynamics on the excited-state potential energy surface of the molecular motor rather than solvent dynamics.

The ultrafast (about 100 fs) quenching of fluorescence may occur by one of two mechanisms, both of which involve excited-state structural relaxation. First, the excited state undergoes radiationless

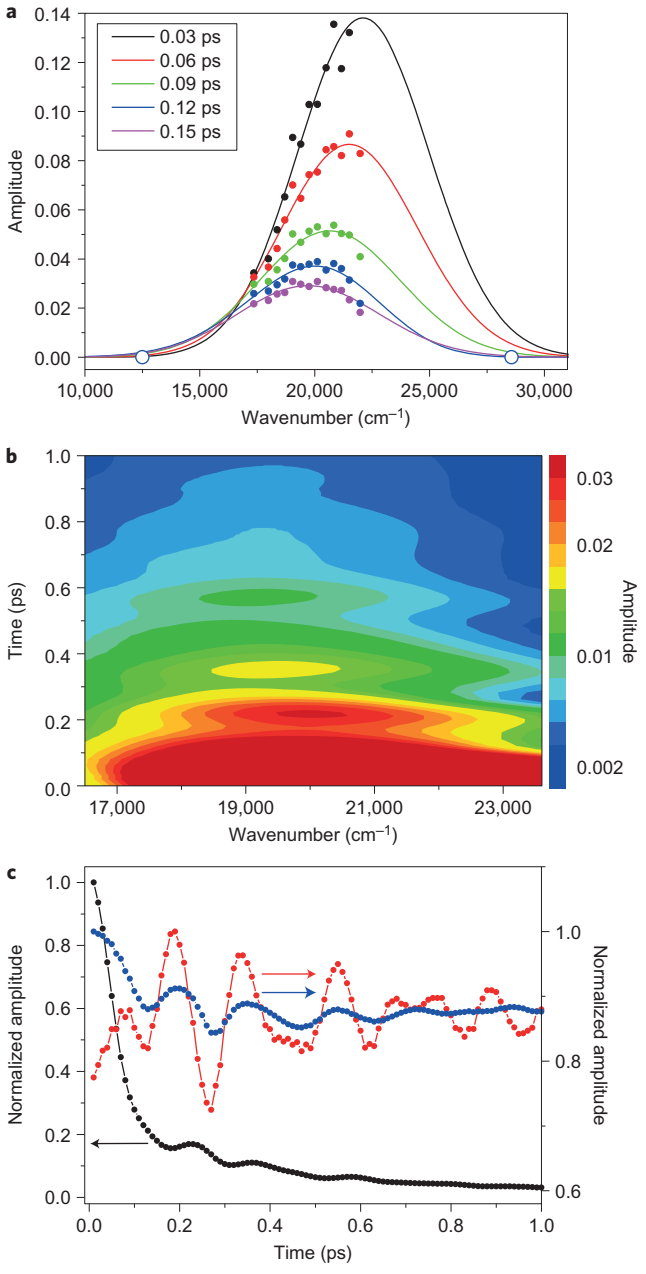

Figure 3 | Excited-state dynamics viewed through the time-dependent emission. a, Time-resolved emission spectra extracted from the deconvoluted wavelength-resolved decay data (points) and fitted to a log-normal function (lines). See Supplementary Tables S1 and S2 for the fitting parameters. **b**, Contour plot of the time-resolved deconvoluted emission, in which the ultrafast decay and the oscillatory feature are evident. **c**, Time-dependent integrated area (black, left amplitude axis), mean frequency (blue, right amplitude axis) and width of the time-resolved spectra (red, right amplitude axis). It was established that the behaviour reported in (**a**)–(**c**) was independent of the fitting function used (see Supplementary Section S2 and Fig. S3).

decay directly back to the ground state, such as may occur through internal conversion at a conical intersection between the ground- and excited-state potential energy surfaces. For such an ultrafast decay the conical intersection must be reached via a barrierless structure change. Alternatively, fluorescence may be quenched by structural relaxation on the excited-state surface, in which the population evolves away from the emissive Franck–Condon excited state to a conformation with a low or zero fluorescence-transition moment; this dark (or near-dark) state may then decay to the ground state on a longer timescale. The latter mechanism is more consistent with the observed non-single exponential decay of the integrated fluorescence intensity, where the fast component reflects the light to dark structural evolution and the slower component the rate of radiationless decay of the dark state back to the ground state. A non-exponential population relaxation for the direct-decay mechanism is expected only if there is an initial distribution of ground-state structures.

Wave-packet dynamics. The second notable feature in the time-domain data is the strong oscillation in the time-resolved emission, which is observed in both the time-dependent integrated intensity and the mean frequency of the time-resolved spectrum (Fig. 3b,c). An oscillation in the mean frequency may arise when a Franck–Condon active vibration is displaced between the ground and excited electronic states. Thus, ultrafast electronic excitation launches a wave packet on the excited-state surface that oscillates with the frequency of the mode in the excited state[16,19]. In this case the phase of the oscillation observed is expected to shift by π when the observation wavelength is changed from the blue to the red edge of the emission spectrum, and its amplitude is expected to be greatest on the rising and falling edges of the spectrum. The oscillation observed in the time-resolved integrated intensity shows that the Franck–Condon active mode must also be coupled to the transition moment; that is, the motion excited in the upper state modulates the probability as well as the energy of fluorescence. In this case the amplitude of the entire spectrum is modulated and there is no phase shift with observation wavelength[20]. Although the very broad emission spectrum (Fig. 2a) precludes fluorescence up-conversion observations across the entire spectrum, within the range of wavelengths investigated an approximately $\pi/2$ phase shift is observed as we move across the spectrum (Supplementary Information Table S2). However, the amplitude of the oscillation is significantly stronger around the maximum in the emission spectrum than on the edges. These data suggest that, at least for the dominant lower-frequency mode, the modulation arises both from coupling between the excited-state vibration and the transition moment and from modulation of the frequency of the electronic transition.

Excited-state structural dynamics. To assign the observed ultrafast fluorescence decay and oscillatory dynamics we turn to existing quantum chemical and molecular dynamics simulations of the photoisomerization of carbon–carbon double bonds. These models, which have a long history, typically invoke motion on two coordinates in the excited electronic state, which leads to a conical intersection between the excited and ground electronic states, where ultrafast internal conversion may occur[21–23]. Calculations reported previously[11] on a motor analogous to **1** suggested that π–π^* electronic excitation is followed by simultaneous twisting about the C9–C1′ double bond and substantial pyramidalization at the stator–axle linkage (C9). We suggest that the experimentally observed oscillations reflect Franck–Condon excitation of the inversion (pyramidalization) mode at C9. Motion along the pyramidalization coordinate coupled with C9–C1′ rotation takes the molecule out of the strongly emissive Franck–Condon region to a point on the potential surface that has a significantly reduced fluorescence-transition moment; the nuclear motions proposed and the relevant potential energy surface are illustrated in Fig. 4. This initial motion leads to the observed ultrafast decay of fluorescence. The molecule then decays from this dark state back to the ground state on a timescale of approximately 1 ps, presumably through an S_0–S_1 conical intersection. In the earlier calculations[11] on the analogue of **1**, two conical intersections were identified on the S_1 potential energy surface as a function of the twist and pyramidalization coordinates, both lying slightly above the

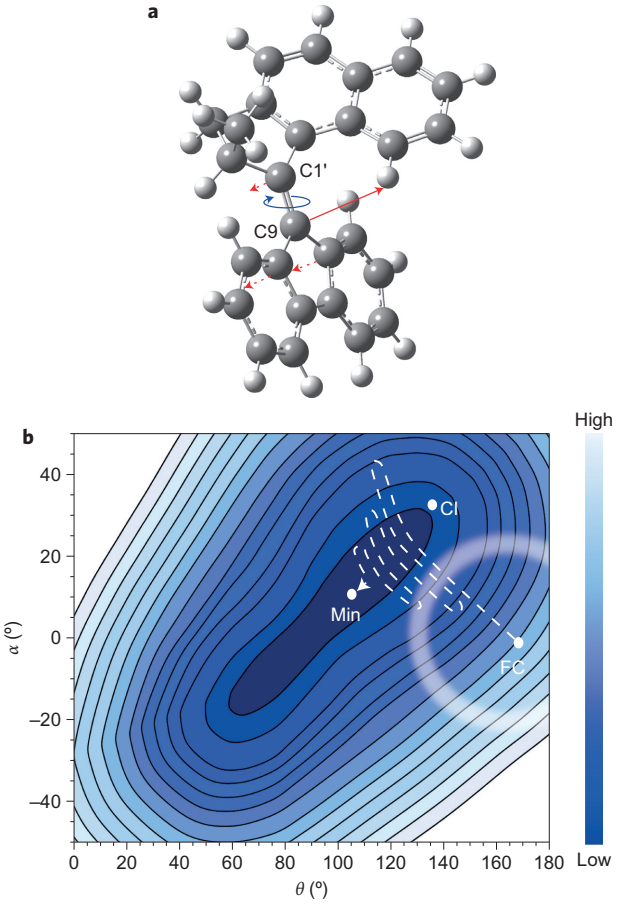

Figure 4 | Schematic model for the excited-state dynamics of 1. **a**, Illustration of the pyramidalization (red arrows) and twisting (blue arrow) motions proposed to contribute to the photoisomerization. **b**, Schematic representation of the primary dynamics of **1** on the excited-state surface. Excitation places the population in the excited state at the Franck–Condon (FC) point. Ultrafast structural relaxation occurs along the pyramidalization (α) and twist (θ) coordinates on a 100 fs timescale. This coherent motion takes the population out of the bright Franck–Condon region (shown as a diffuse circle), which leads to the observed 100 fs relaxation. The coherent motion of the dominant mode on the upper surface damps, with an approximately 100 fs time constant, which leads to a thermal population about the minimum (Min) on the potential surface. This thermalized population decays to the ground state through a conical intersection (CI) on the picosecond timescale.

minimum energy; these ideas are illustrated in Fig. 4b. In this model, the ultrafast component arises from structural dynamics, which suggests that the 1.7 ps component reported as structural relaxation in earlier transient-absorption experiments[10] on a related molecular motor could be associated with population decay, and the slower component observed there probably reflects vibrational cooling of the hot ground state of the molecular motor. Preliminary transient-absorption studies of **1** reported here (see Supplementary Section S4 and Fig. S4) show that the decay of a transient state that is populated within a few hundred femtoseconds occurs with a 1.5 ± 0.3 ps time constant, consistent with the decay time of the relaxed excited state seen in fluorescence. The earlier calculations[11] on an analogue of **1** mentioned above suggested that the relaxed state is already substantially distorted compared with the Franck–Condon state (Fig. 4a), which suggests that extensive structural change has already occurred in the excited state.

Although the qualitative agreement between the calculations and the experiment is good, the assignment of the 113 cm^{-1} mode to the inversion/pyramidalization coordinate remains speculative. However, there is additional evidence from the damping constants that this mode is involved actively in the primary isomerization (power) stroke of the molecular motor. This low-frequency mode is damped on the sub 100 fs timescale, which is as fast as or faster than the relaxation out of the Franck–Condon region. This is in contrast to the weaker 180 cm^{-1} mode, which has a much longer damping time, suggesting that the latter may simply be a spectator mode, uninvolved in the excited-state dynamics.

We have sought a more definitive assignment of these coherent excited-state modes through resonance Raman spectroscopy (Fig. 5). Although continuous-wave Raman spectroscopy (unlike time-resolved fluorescence) can only yield ground-state frequencies, the observation of a resonance enhancement does reveal modes that are coupled to the optical excitation, and thus points to nuclear motions that are displaced from equilibrium geometry along normal coordinates in the excited state. The resonance Raman spectrum (Fig. 5) does not show modes in the ground state that match exactly the observations in the excited state (Fig. 2b). This is not in itself surprising. It is not, in general, possible to find a direct one-to-one correspondence between ground- and excited-state frequencies, as the widely studied example of *cis*-stilbene, which also undergoes a fast excited-state reaction believed to involve both twisting and pyramidalization, shows[24–26]. However, resonantly enhanced modes near 300 cm^{-1} are observed, one of which is calculated in the present study to involve out-of-plane nuclear displacement around C9 (Fig. 5). It is plausible that such modes are strongly down shifted in frequency in the excited electronic state following a π–π^* transition localized at the C9 axle double bond[11].

The observation of optically excited strongly damped coherent excited-state dynamics is of potential importance to the operation of light-driven molecular motors. That there is room for further optimization of the motor operation is evident from quantum-yield data (Supplementary Section S5 and Fig. S6), which show a

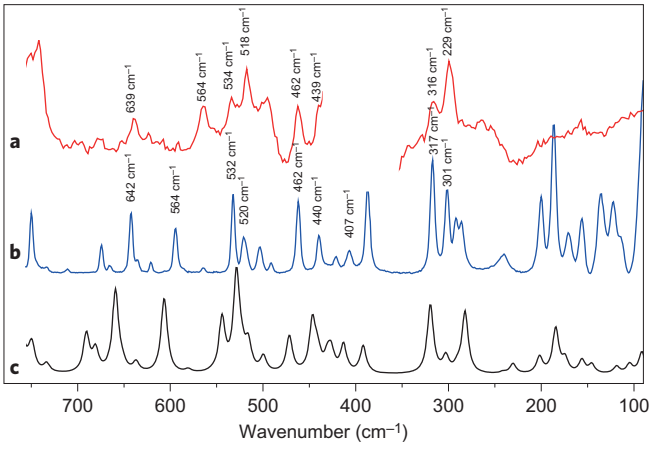

Figure 5 | Comparison of the resonance and off-resonance Raman spectra of 1 with the calculated Raman spectrum. a, The resonance Raman spectrum of **1** in cyclohexane (with the solvent background subtracted) was recorded with 355 nm radiation in a flowing sample cell. Measurements in DCM, although otherwise identical to those in cyclohexane, were not useful as the region of most interest was obscured by the solvent bands. Even in cyclohexane the region between 350 and 450 cm^{-1} was distorted severely by very intense solvent bands. **b**, The off-resonance Raman spectrum recorded for crystalline **1** at 785 nm; compared with (**a**) this reveals resonantly enhanced modes near 300 cm^{-1}. **c**, The calculated (gas phase) Raman spectrum of **1** recovered from density functional theory calculations. The agreement with (**b**) is excellent. Additional bands in (**b**) at low frequency may be assigned to crystal modes. Further information is given in Supplementary Fig. S4.

yield of 0.14. First, the important role for the inversion mode at C9 in the structural dynamics is suggested by both experiment and theory, so synthetic strategies that modulate the electronic structure in the C9–C1′ double bond probably modify the efficiency of operation; we are currently studying a series of derivatives of **1** to further probe this dependence. Second, the observation of coherent dynamics in a mode that is involved actively in the excited-state reaction coordinate raises the possibility that coherent control schemes can be exploited to drive the reaction in a specific direction[17,27,28]. Coherent control of photochemical reactivity using chirped pulses was discussed in a number of cases, which include a theory-based proposal for molecular motors and an experimental demonstration on the biological photoswitch in the retinal visual pigment bacteriorhodopsin[28–30]. However, its application has proved to be limited to very few examples, because of both the ultrafast dephasing times characteristic of electronic states in fluid media at room temperature and the difficulty of optically accessing the chemically important modes. The present data suggest that coherent excitation schemes could be applied to control the reaction of light-driven molecular motors, at least on the sub 100 fs timescale of the dephasing time associated with the active mode. Within this limitation, appropriately shaped pulses could be used to steer the excited state towards (or away from) the conical intersection, and thus optically control the efficiency of motor rotation.

Methods

A titanium sapphire laser that delivered 18 fs pulses at 800 nm with an 80 MHz repetition rate was used, and the two frequencies required by the experiment were obtained through second-harmonic generation. The ultrafast up-conversion apparatus is described in detail elsewhere[12]. Essentially, up-conversion is an ultrafast sampling method in which solute fluorescence excited by an ultrashort 400 nm pulse is focused into a nonlinear crystal, where it is mixed with an ultrashort 800 nm pulse. The intensity of the resulting sum-frequency signal is linearly proportional to the intensity of the fluorescence at the instant of arrival of the 800 nm pulse. The fluorescence decay is recorded by scanning the arrival time of the 800 nm pulse. Time resolution is limited only by the cross-correlation width of the 400 nm and 800 nm pulses. The time resolution was optimized by compensating for the pulse-broadening effects of transmission through dispersive optics and by the use of mainly reflective optics[12,31]. Wavelength selection was by a monochromator and through angle tuning of the nonlinear crystal. Data analysis was by deconvolution using up-converted solvent Raman scattering as the instrument response; fitting was optimized using a genetic algorithm and judged by the distribution of residuals (see Supplementary Sections S1 and S2 and Fig. S2). Further experimental information on Raman and transient absorption is presented in the Supplementary Information.

Samples of **1** in DCM were 0.5 mM in concentration. The preparation and characterization of **1** are described elsewhere[5,32].

Received 31 January 2012; accepted 26 March 2012; published online 6 May 2012

References

1. Kay, E. R., Leigh, D. A. & Zerbetto, F. Synthetic molecular motors and mechanical machines. *Angew. Chem. Int. Ed.* **46,** 72–191 (2007).
2. Balzani, V., Credi, A. & Venturi, M. Light powered molecular machines. *Chem. Soc. Rev.* **38,** 1542–1550 (2009).
3. Koumura, N., Zijlstra, R. W. J., van Delden, R. A., Harada, N. & Feringa, B. L. Light-driven monodirectional molecular rotor. *Nature* **401,** 152–155 (1999).
4. Koumura, N., Geertsema, E. M., van Gelder, M. B., Meetsma, A. & Feringa, B. L. Second generation light-driven molecular motors. Unidirectional rotation controlled by a single stereogenic center with near-perfect photoequilibria and acceleration of the speed of rotation by structural modification. *J. Am. Chem. Soc.* **124,** 5037–5051 (2002).
5. Vicario, J., Meetsma, A. & Feringa, B. L. Controlling the speed of rotation in molecular motors. Dramatic acceleration of the rotary motion by structural modification. *Chem. Comm.* 5910–5912 (2005).
6. van Delden, R. A. *et al.* Unidirectional molecular motor on a gold surface. *Nature* **437,** 1337–1340 (2005).
7. Pollard, M. M., Klok, M., Pijper, D. & Feringa, B. L. Rate acceleration of light-driven rotary molecular motors. *Adv. Funct. Mater.* **17,** 718–729 (2007).
8. Klok, M. *et al.* MHz unidirectional rotation of molecular rotary motors. *J. Am. Chem. Soc.* **130,** 10484–10485 (2008).
9. Klok, M., Browne, W. R. & Feringa, B. L. Kinetic analysis of the rotation rate of light-driven unidirectional molecular motors. *Phys. Chem. Chem. Phys.* **11,** 9124–9131 (2009).
10. Augulis, R., Klok, M., Feringa, B. L. & van Loosdrecht, P. H. M. Light-driven rotary molecular motors: an ultrafast optical study. *Phys. Status Solidi C* **6,** 181–184 (2009).
11. Kazaryan, A. *et al.* Understanding the dynamics behind the photoisomerization of a light-driven fluorene molecular rotary motor. *J. Phys. Chem. A* **114,** 5058–5067 (2010).
12. Heisler, I. A., Kondo, M. & Meech, S. R. Reactive dynamics in confined liquids: ultrafast torsional dynamics of auramine O in nanoconfined water in aerosol OT reverse micelles. *J. Phys. Chem. B* **113,** 1623–1631 (2009).
13. Glasbeek, M. & Zhang, H. Femtosecond studies of solvation and intramolecular configurational dynamics of fluorophores in liquid solution. *Chem. Rev.* **104,** 1929–1954 (2004).
14. Morales, A. R., Belfield, K. D., Hales, J. M., Van Stryland, E. W. & Hagan, D. J. Synthesis of two-photon absorbing unsymmetrical fluorenyl-based chromophores. *Chem. Mater.* **18,** 4972–4980 (2006).
15. Nakamura, T., Takeuchi, S., Suzuki, N. & Tahara, T. Revised steady-state fluorescence spectrum and nature of the reactive *S*(1) state of *cis*-stilbene in solution. *Chem. Phys. Lett.* **465,** 212–215 (2008).
16. Mokhtari, A., Chebira, A. & Chesnoy, J. Subpicosecond fluorescence dynamics of dye molecules. *J. Opt. Soc. Am. B* **7,** 1551–1557 (1990).
17. Hauer, J., Buckup, T. & Motzkus, M. Enhancement of molecular modes by electronically resonant multipulse excitation: further progress towards mode selective chemistry. *J. Chem. Phys.* **125,** 061101 (2006).
18. Klok, M., Janssen, L., Browne, W. R. & Feringa, B. L. The influence of viscosity on the functioning of molecular motors. *Faraday Discuss.* **143,** 319–334 (2009).
19. Pollard, W. T., Lee, S. Y. & Mathies, R. A. Wave packet theory of dynamic absorption-spectra in femtosecond pump-probe experiments. *J. Chem. Phys.* **92,** 4012–4029 (1990).
20. Rubtsov, I. V. & Yoshihara, K. Vibrational coherence in electron donor–acceptor complexes. *J. Phys. Chem. A* **103,** 10202–10212 (1999).
21. Sanchez-Galvez, A. *et al.* Ultrafast radiationless deactivation of organic dyes: evidence for a two-state two-mode pathway in polymethine cyanines. *J. Am. Chem. Soc.* **122,** 2911–2924 (2000).
22. Hahn, S. & Stock, G. Quantum-mechanical modeling of the femtosecond isomerization in rhodopsin. *J. Phys. Chem. B* **104,** 1146–1149 (2000).
23. Levine, B. G. & Martinez, T. J. Isomerization through conical intersections. *Annu. Rev. Phys. Chem.* **58,** 613–634 (2007).
24. Myers, A. B. & Mathies, R. A. Excited-state torsional dynamics of *cis*-stilbene from resonance Raman intensities. *J. Chem. Phys.* **81,** 1552–1558 (1984).
25. Ishii, K., Takeuchi, S. & Tahara, T. A 40-fs time-resolved absorption study on *cis*-stilbene in solution: observation of wavepacket motion on the reactive excited state. *Chem. Phys. Lett.* **398,** 400–406 (2004).
26. Takeuchi, S. *et al.* Spectroscopic tracking of structural evolution in ultrafast stilbene photoisomerization. *Science* **322,** 1073–1077 (2008).
27. Hauer, J., Buckup, T. & Motzkus, M. Quantum control spectroscopy of vibrational modes: comparison of control scenarios for ground and excited states in beta-carotene. *Chem. Phys.* **350,** 220–229 (2008).
28. Prokhorenko, V. I. *et al.* Coherent control of retinal isomerization in bacteriorhodopsin. *Science* **313,** 1257–1261 (2006).
29. Flores, S. C. & Batista, V. S. Model study of coherent-control of the femtosecond primary event of vision. *J. Phys. Chem. B* **108,** 6745–6749 (2004).
30. Perez-Hernandez, G., Pelzer, A., Gonzalez, L. & Seideman, T. Biologically inspired molecular machines driven by light. Optimal control of a unidirectional rotor. *New J. Phys.* **12,** 1–24 (2010).
31. Rhee, H. & Joo, T. Noncollinear phase matching in fluorescence upconversion. *Opt. Lett.* **30,** 96–98 (2005).
32. Pollard, M. M., Meetsma, A. & Feringa, B. L. A redesign of light-driven rotary molecular motors. *Org. Biomol. Chem.* **6,** 507–512 (2008).

Acknowledgements

This work was supported by the Engineering and Physical Sciences Research Council (EP/E010466), European Research Council (ERC) Starting Grant (279549; W.R.B.) and ERC Advanced Investigator Grant (227897; A.C., B.L.F.). J.C. was supported by a University of East Anglia studentship.

Author contributions

S.R.M., B.L.F. and W.R.B. conceived and designed the experiments. J.C. and K.A. performed the time-resolved experiments, I.H. constructed the up-conversion apparatus, A.C. and B.L.F. designed and synthesized **1**, J.C. and A.C. performed the steady-state electronic spectroscopy, J.C. and I.H. analysed the time-resolved data, A.C. performed the density functional theory calculations, W.R.B obtained and analysed the Raman data, S.R.M. wrote the paper and all the authors commented and contributed to the writing of the manuscript.

Additional information

The authors declare no competing financial interests. Supplementary information and chemical compound information accompany this paper at www.nature.com/naturechemistry. Reprints and permission information is available online at http://www.nature.com/reprints. Correspondence and requests for materials should be addressed to B.L.F. and S.R.M.